AUTHOR QUERY FORM

Journal: TSF **Article Number: 28466**	**Please e-mail or fax your responses and any corrections to:** **E-mail:** corrections.esil@elsevier.spitech.com **Fax: +1 619 699 6721**

Dear Author,

Any queries or remarks that have arisen during the processing of your manuscript are listed below and highlighted by flags in the proof. Please check your proof carefully and mark all corrections at the appropriate place in the proof (e.g., by using on-screen annotation in the PDF file) or compile them in a separate list.

For correction or revision of any artwork, please consult http://www.elsevier.com/artworkinstructions.

No queries have arisen during the processing of your article.

Thank you for your assistance.

SnS thin-films by RF sputtering at room temperature

Katy Hartman [a,*], J.L. Johnson [b], Mariana I. Bertoni [a], Daniel Recht [c], Michael J. Aziz [c], Michael A. Scarpulla [b], Tonio Buonassisi [a]

[a] *Massachusetts Institute of Technology, 77 Massachusetts Ave. Bldg 35, Cambridge, MA 02139, USA*
[b] *University of Utah, Merrill Engineering Building, 50 Central Campus Dr., Salt Lake City, UT 84112, USA*
[c] *Harvard School of Engineering and Applied Sciences, 29 Oxford St., Cambridge, MA 02138, USA*

ARTICLE INFO

Available online xxxx

Keywords:
Tin sulfide
Tin monosulfide
RF sputtering
Solar cells
Photovoltaics

ABSTRACT

Tin monosulfide (SnS) is of interest as a potential solar cell absorber material. We present a preliminary investigation of the effects of sputtering conditions on SnS thin-film structural, optical, and electronic properties. Films were RF sputtered from an SnS target using an argon plasma. Resistivity, stoichiometry, phase, grain size and shape, bandgap, and optical absorption coefficient can be varied by modifying argon pressure for a fixed deposition time. Most films have an indirect bandgap in the range of 1.08–1.18 eV. XRD patterns confirmed the films as mostly crystalline, and grain morphology was examined using profile and surface SEM images.

© 2010 Published by Elsevier B.V.

1. Introduction

Tin monosulfide (SnS) is a promising solar cell absorber material due to its high absorption coefficient of $\sim 10^4$–10^5 cm^{-1} [1] and near-optimal direct bandgap of 1.3 eV [2]. The high natural abundance of tin and sulfur could potentially enable scaling of SnS photovoltaics manufacturing to terawatt levels [3]. The current record efficiency of an SnS photovoltaic device is only 1.3% [2], which is substantially less than the theoretical maximum efficiency of 32% [4]. Fundamental research is necessary to explore the reasons for this low performance, and determine the ultimate potential of this material.

Tin sulfide thin-films have been deposited by methods such as thermal evaporation [5], chemical bath deposition [6], spray pyrolysis [2], sulfurization [7], electrodeposition [8], AP-CVD [9] and electron-beam evaporation [10]. Despite the widespread use of sputtering for deposition of other materials, the application of sputtering to SnS remains limited. While sputtering has several advantages, the sputtering of metal sulfides has some distinct challenges, such as the volatility of sulfur and the difficulty of precise target composition control.

To date, there are sparse reports of SnS sputtering in the literature, and these explore a limited range of deposition conditions. Guang-Pu et al. [11] reported a cursory study of RF sputtering of tin sulfide in 1994, while Shinichi and Shigetoshi [12] reported SnS thin-films reactively sputtered using a pure tin target and an H$_2$S/Ar gas mixture.

This manuscript presents a preliminary exploration of RF sputtering from an SnS target. We investigate the effect of various sputtering conditions on SnS thin-film structural, optical, and electronic properties.

2. Materials and methods

2.1. Sputtering conditions

Depositions were performed using a magnetron sputtering system located at the University of Utah. High vacuum was achieved using a turbomolecular pump and a liquid nitrogen cold trap. RF sputtering was performed with an argon plasma, at a substrate distance of 16.5 cm, with a horizontal sputtering geometry.

A 7.62 cm (3 in.) diameter SnS target was purchased from Plasmaterials. The original powder SnS material was 99.95% pure, however compositional analysis performed via X-ray fluorescence (XRF) microprobe revealed a sulfur-rich uniform final target composition of Sn: 39 at.% and S: 61 at.% (± 2 at.%).

SnS thin-films were deposited on soda-lime glass microscope slides. All substrates were manually scrubbed using detergent, then rinsed in deionized water, acetone, methanol, and isopropyl alcohol. Substrates were then exposed to ultraviolet-generated ozone for 2 min. All samples had a deposition time of 60 min, a substrate rotation of 18 rpm, a base pressure range of 1–6×10^{-7} Torr, and an initial substrate temperature of 25 °C. Reflected power was maintained within a 0–2 W range. Four SnS thin-films were created with varying argon pressures and an approximately constant power.

---

* Corresponding author.
   E-mail address: khartman@alum.mit.edu (K. Hartman).

At this power level, the substrate temperature increased to at least 80 °C over the 60 min deposition.

2.2. Characterization methods

X-ray diffraction measurements were taken using Cu K_α radiation ($\lambda = 1.54$ Å). The data was collected in the Bragg–Brentano configuration, with a constant irradiated area. Scanning electron micrographs of the film surface were taken on a Zeiss Supra 55VP field-emission SEM. Film thickness measurements were taken using a KLA-Tencor P-16 surface profilometer. The error on these measurements is estimated to be ± 30 Å.

The wavelength-dispersive spectroscopy (WDS) was performed on all samples, using a JEOL JXA-8200 Superprobe with a tungsten filament, an acceleration voltage of 15 kV, 10 nA beam current, and 50 μm spot size. The standards used for compositional analysis were pure Sn, NiS, and Fe_2O_3 for tin, sulfur and oxygen respectively. The raw data were corrected using matrix (ZAF) corrections and an excitation volume correction that assumed a homogeneous SnS thin-film on a semi-infinite SiO_2 substrate [13]. Additionally, we assume that all oxygen signals originate from the substrate. The WDS measurements were validated by two SnS thin-film samples, which were also analyzed using the Rutherford backscattering (RBS) at Evans Analytical Group. The errors for WDS and RBS range from 0.2 to 0.5 at.% for tin, and 0.2 to 1 at.% for sulfur. For both WDS and RBS measurements, the assumption of a homogeneous film of constant density is a source of additional error. These SnS films are highly heterogeneous, thus the absolute stoichiometry values are likely affected by a higher error than specified. However, trends from sample to sample are likely accurate.

The four-point-probe resistivity measurements were performed on all samples using a Keithley 4200 and osmium tips. Resistivities were consistent from region to region on a given sample to within 20% of the reported values. This uncertainty was likely due to the variations in film thickness and the noise inherent in high resistivity measurements. Optical measurements were performed at room temperature using a Perkin Elmer Lambda 950 UV/Vis/NIR spectrophotometer with an 8° incident beam. The specular reflectivity measurements were referenced using a silver mirror. The absorption coefficient values were calculated from experimental transmission and reflection data.

3. Results and discussion

3.1. Phase identification

XRD data in Fig. 1 show that all peaks in Samples A through C are matched to the orthorhombic phase of SnS (PDF Card # 00-039-0354) [14]. The intensity of the 002 peak relative to the 101 and 111 peaks decreases from Samples A to C, indicating a change in the preferred growth orientation of these films. We observe small shifts in peak positions for certain diffraction conditions, confirmed by XRD measurements taken using parallel-beam optics. In all samples, the 110 and 042 peaks are shifted by + 0.3° and − 0.3° 2θ, respectively, half the value at full width at half maximum. Cell refinement suggests that these systematic peak shifts cannot be explained by the simple distortion of the SnS unit cell.

In Sample D, the 2θ-shift of the two main XRD peaks away from SnS peaks 101 and 111 indicates that this film may contain a different phase. The Sample D peak at 30.9° 2θ matches well to the 310 peak in the Sn_2S_3 phase (PDF Card # 00-014-0619) [14].

3.2. Grain morphology

Samples A–C exhibit an elongated grain shape when imaged in plain view at the film surface (Fig. 2). The "rice-shaped" grains in
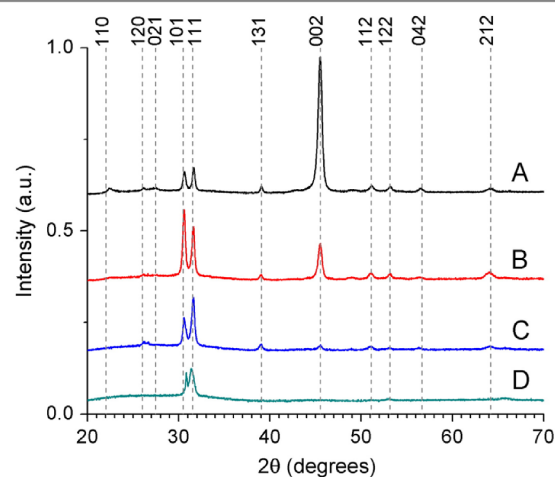

Fig. 1. X-ray diffraction data for the four samples depicted in Table 1. Dashed lines represent SnS diffraction peak positions listed by PDF # 00-039-0354 (space group: Pbnm; a = 4.329 Å, b = 11.192 Å, c = 3.984 Å). The data indicate that Samples A, B, and C are SnS. (For interpretation of the references to color in this figure legend, the reader is referred to the web version of this article.)

these images appear to be composed of elongated nanocrystallites less than 25 nm in thickness. The shape of these nanocrystallites closely follows that of the elongated grain. The grain length (Table 1), as measured along the long axis of the grains, is comparable to that of other SnS films produced by thermal evaporation by Devika et al. with a substrate heating of 300 °C [15]. Cross-sectional SEM images suggest that the films are fairly porous (Fig. 3). Gaps appear between grains, which extend through most of the film thickness, indicating elevated film porosity.

An apparent trend of the decreasing grain length with the increasing argon pressure for Samples A through C is observed in Fig. 2. Sample D exhibits a qualitatively distinct grain structure from the other films. Grains on the order of 30 nm lack the characteristic elongated shape of Samples A–C, but maintain the sub-grain nanocrystallite structure.

The trend of a decreasing grain size in Samples A–C may not be due solely to an increasing argon sputtering pressure. In our experiments, this growth parameter is convoluted with changes in film thickness and growth rate, two parameters known to affect grain size in other material systems.
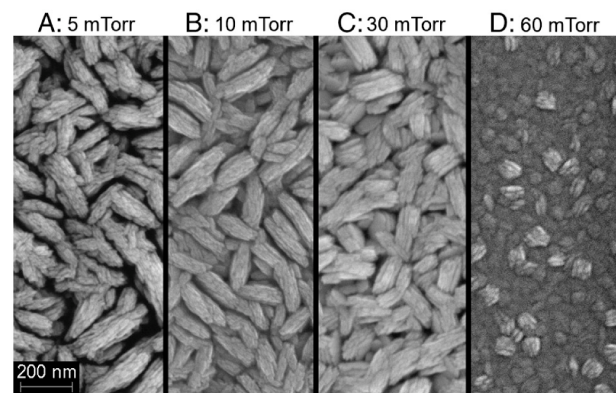

Fig. 2. Plain view SEM images of representative regions of four samples listed in Table 1. Samples A–C exhibit an elongated grain morphology with evident porosity, while Sample D exhibits a less porous, equiaxed structure. Intragranular nanocrystallites are also observed.

Table 1

Sputtering deposition parameters (above) and measured material characteristics (below) for four tin sulfide thin-films. Sputtering time was 60 min.

Sample label	A	B	C	D
Argon pressure (mTorr)	5	10	30	60
Power (W)	150	160	150	150
Film thickness (μm)	1.58	1.06	0.46	0.23
Indirect bandgap (eV)	1.18	1.12	1.08	–
Sn/S ratio	1.07	1.08	1.10	1.02
Grain length (nm)	198	195	100	30
Resistivity (Ω cm)	1100	13,900	97,000	33,000

3.3. Stoichiometry

The resistivity of binary semiconductors is known to be strongly dependent on small deviations in stoichiometry (*e.g.* GaAs). We observe a slightly increasing Sn/S ratio from Samples A to C (Table 1). Sample D, which demonstrates a different film morphology and XRD signature, exhibits a lower Sn/S ratio. In Samples A–C, we also note a trend of an increasing Sn/S ratio with a decreasing thickness. A similar trend was observed for SnS films deposited by thermal evaporation at 300 °C [15]. The target had an Sn/S ratio of 0.64, but the resulting films are tin-rich, suggesting that sulfur was lost during the deposition process.
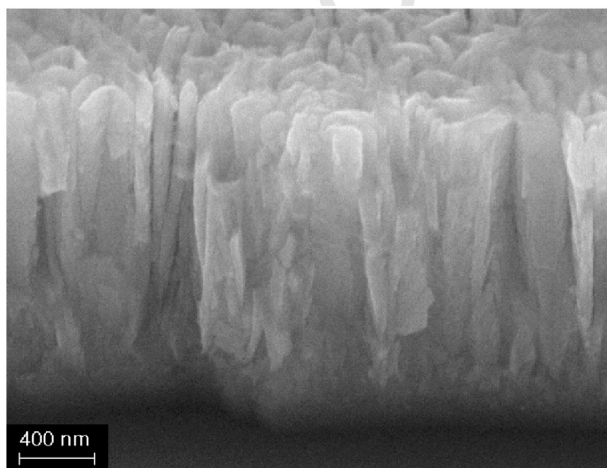
3.4. Resistivity

In-plane resistivity measurements (Table 1) increase from Samples A to C. Sample D, which exhibits a markedly different XRD signature, film morphology, and stoichiometry, exhibits a lower resistivity than Sample C. We note the high resistivity values for all samples, which would limit the efficiency in a photovoltaic device.

The cause of the high resistivity values is not currently known. The observed general trend of the resistivity increase with the decrease in thickness may be influenced by surface roughness, interface and grain boundary scattering, percolation effects due to porosity, and carrier concentration changes due to off-stoichiometry. Further work is needed to study these effects and improve electrical transport.

3.5. Absorption coefficient and optical bandgap

For all samples, we observe an absorption coefficient (α) in the 10^3–10^4 cm^{-1} range within a few hundred meV from the absorption onset (Fig. 4a). Samples A–C exhibit qualitatively similar α vs. photon energy behavior, and the absolute value appears to increase from A to C. The absorption coefficient behavior for Sample D is distinct from that of Samples A–C.
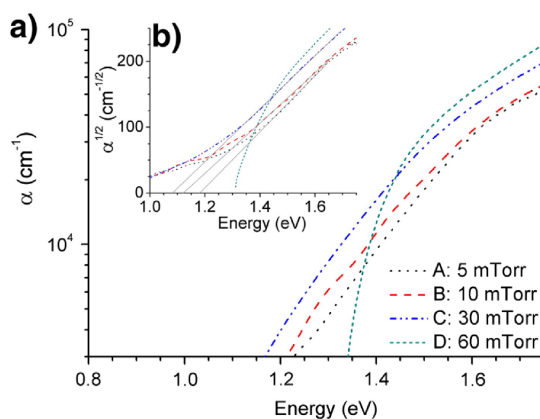
In Fig. 4b, a linear portion for Samples A–C is apparent on the $\alpha^{1/2}$ vs. photon energy diagram, indicating that the indirect bandgap relation is applicable (Table 1) [16]. A satisfactory linear fit for a direct bandgap estimation cannot be made for any sample when α^2 is plotted vs. photon energy. These results appear to be consistent with the reports of other authors who compute indirect bandgaps in the range of 1.0 to 1.3 eV for SnS single crystals [17] and thin-films grown by thermal evaporation [18], chemical bath deposition [19], and electron-beam evaporation [10]. Nevertheless, there exists a discrepancy in the literature concerning this point. Other reports of films grown by thermal evaporation [1,5], the SILAR method [20], spray pyrolysis [2], and sputtering [11] use direct bandgap fitting to obtain values for SnS thin-films typically in the range of 1.3–1.7 eV.

The absorption coefficient vs. photon energy of Sample D does not conform to either direct or indirect bandgap fitting. If Sample D is a multi-phase mixture, as suggested by XRD and stoichiometry measurements, then we could not expect to observe a simple behavior.

4. Summary

We presented an exploratory investigation into SnS sputtering for thin-film solar cell applications. The structural, optical and electronic properties of these films are observed to vary when growth is conducted at different argon pressures with a constant deposition time. The XRD analysis indicates that the preferential film orientation changes systematically between our samples, which may bear relevance to solar cell fabrication due to the anisotropic carrier transport properties of SnS [17]. The observed variation in grain length and preferred grain orientation may be due to the differences in growth rate, argon pressure, and/or film thickness. Future experiments will seek to decouple these variables and identify the dominant factor(s) and relevant growth mechanisms.

Samples A–C are determined to have indirect bandgaps in the range of 1.08–1.18 eV, while Sample D cannot be characterized as either direct or indirect with the existing data. The measured absorption coefficients and conductivities are slightly low for use in thin-film solar cells. However, these values could be improved by annealing and densification. Further work will focus on improving SnS film quality for use in solar cells.

Fig. 3. Cross-sectional SEM image of a cleaved section of Sample A acquired at 45° relative to the surface showing the entire film thickness. Within 200–300 nm of the substrate a high-density, small-grained morphology can be observed. Above 300 nm from the interface, directional grain growth can be observed, albeit with some porosity.

Fig. 4. Optical absorption measurements: (a) absorption coefficient vs. photon energy and (b) a plot using the indirect bandgap model, proportional to $\alpha^{1/2}$. Samples A, B, and C have indirect bandgaps. (For interpretation of the references to color in this figure legend, the reader is referred to the web version of this article.)

References

[1] H. Noguchi, A. Setiyadi, H. Tanamura, T. Nagatomo, O. Omoto, Sol. Energy Mater. Sol. Cells 35 (1994) 325.
[2] K.T. Ramakrishna Reddy, N. Koteeswara Reddy, R.W. Miles, Sol. Energy Mater. Sol. Cells 90 (2006) 3041.
[3] G.B. Haxel, J.B. Hedrick, G.J. Orris, Rare Earth Elements-Critical Resources for High Technology, US Geological Survey, 2010, http://geopubs.wr.usgs.gov/fact-sheet/fs087-02/.
[4] W. Shockley, H.J. Queisser, J. Appl. Phys. 32 (3) (1961) 510.
[5] O.E. Ogah, G. Zoppi, I. Forbes, R.W. Miles, Thin Solid Films 517 (2009) 2485.
[6] P. Pramanik, P.K. Basu, S. Biswas, Thin Solid Films 150 (1987) 269.
[7] M. Sugiyama, K. Miyauchi, T. Minemura, K. Ohtsuka, K. Noguchi, H. Nakanishi, Jpn. J. Appl. Phys. 47 (6) (2008) 4494.
[8] K. Takeuchi, M. Ichimura, E. Arai, Y. Yamazaki, Sol. Energy Mater. Sol. Cells 75 (2003) 427.
[9] L.S. Price, I.P. Parkin, T.G. Hibbert, K.C. Molloy, Chem. Vap. Deposition 4 (6) (1998) 222.
[10] A. Tanuševski, D. Poelman, Sol. Energy Mater. Sol. Cells 80 (3) (2003) 297.
[11] W. Guang-Pu, Z. Zhi-Lin, Z. Wei-Ming, G. Xiang-Hong, C. Wei-Qun, H. Tanamura, M. Yamaguchi, H. Noguchi, T. Nagatomo, O. Omoto, Proceedings of the 1st IEEE World Conference on Photovoltaic Energy Conversion, Honolulu, U.S.A., Dec 5–9, 1994, p. 365.
[12] K. Shinichi, S. Shigetoshi, Japanese Patent # 08-176814, 9 July 1996.
[13] R.A. Waldo, in: D.E. Newbury (Ed.), Microbeam Analysis, San Francisco Press, Inc., San Francisco, 1988, p. 310.
[14] Powder Diffraction File, International Centre for Diffraction Data, Newtown Square, PA, 2009.
[15] M. Devika, N. Koteeswara Reddy, K. Ramesh, R. Ganesan, K.R. Gunasekhar, E.S.R. Gopal, K.T. Ramakrishna Reddy, J. Electrochem. Soc. 154 (2) (2007) H67.
[16] M. Fox, Optical Properties of Solids, Oxford University Press, New York, 2001.
[17] W. Albers, C. Haas, F. van der Maesen, J. Phys. Chem. Solids 15 (1960) 306.
[18] J.B. Johnson, H. Jones, B.S. Latham, J.D. Parker, R.D. Engelken, C. Barber, Semicond. Sci. Technol. 14 (1999) 501.
[19] R.D. Engelken, H.E. McCloud, C. Lee, M. Slayton, H. Ghoreishi, J. Electrochem. Soc. 134 (11) (1987) 2696.
[20] B. Ghosh, M. Das, P. Banerjee, S. Das, Appl. Surf. Sci. 254 (2008) 6436.